Ultrasonics Sonochemistry 118 (2025) 107381

Contents lists available at ScienceDirect

Ultrasonics Sonochemistry

journal homepage: www.elsevier.com/locate/ultson

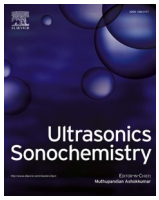

Ca^{2+} sonotransfer into breast cancer cells in a suspension, 3-D spheroid and subcutaneous tumor models☆

Martynas Maciulevičius [a,b,c,*], Reda Rulinskaitė [a,c], Lukas Giedrimas [a], Rūta Palepšienė [a,c], Paulius Ruzgys [a], Rytis Jurkonis [d], Mindaugas Tamošiūnas [e], Renaldas Raišutis [c,f], Kristine Saleniece [g], Saulius Šatkauskas [a]

[a] Research Institute of Natural and Technological Sciences, Vytautas Magnus University, Universiteto 10, Akademija, Kaunas District LT-53361, Lithuania
[b] Department of System Analysis, Faculty of Informatics, Vytautas Magnus University, Universiteto str. 10-213, 53361 Akademija, Kaunas District, Lithuania
[c] Ultrasound Research Institute, Kaunas University of Technology, K. Baršausko st. 59, LT-51423 Kaunas, Lithuania
[d] Biomedical Engineering Institute, Kaunas University of Technology, K. Baršausko st. 59, LT-51423 Kaunas, Lithuania
[e] University of Latvia, Institute of Atomic Physics and Spectroscopy, Jelgavas st. 3, Rīga LV-1004, Latvia
[f] Department of Electrical Power Systems, Faculty of Electrical and Electronics Engineering, Kaunas University of Technology, Studentų st. 48, LT-51367 Kaunas, Lithuania
[g] Faculty of Medicine, University of Latvia, Jelgavas str. 3, LV-1004 Riga, Latvia

ARTICLE INFO

Keywords:
Calcium
Bleomycin
Sonoporation
Spheroids
4T1 cells
Breast cancer

ABSTRACT

Calcium-based treatments have gained considerable attention in the field of electroporation, primarily, due to their comparable efficacy to conventional electro-chemotherapy. However, their applications in sonoporation remain under-investigated, despite its high potential for site-specific and temporally-controlled drug delivery.

Current study examines the curative potential of calcium sonoporation across multiple experimental models, including: i) cell suspension, ii) 3-D spheroid culture and iii) subcutaneous murine breast cancer tumors. Murine breast cancer is an established analogue of stage IV human breast cancer. For comparison, parallel experiments, using classical anticancer drug bleomycin were performed.

Ca^{2+} sonoporation efficiently enhanced 4 T1 cell death in a suspension in the absence of microbubbles, under relatively low acoustic pressure (100–200 kPa). In contrast, efficient spheroid growth reduction required microbubble-mediated inertial cavitation at higher (700 kPa) acoustic pressure.

In vivo, Ca^{2+} sonoporation demonstrated similar tumor growth reduction as bleomycin sonoporation. Both treatments reduced tumor growth from the third day after the onset of treatment. Successful cancer treatment was achieved even at lower values of cavitation dose metrics.

Our study presents a multi-level validation of Ca^{2+} sonoporation as an effective treatment strategy for murine breast cancer. Importantly, complete tumor eradication and prolonged animal survival up to one month were observed even at significantly reduced cavitation activity, indicating clinical safety of the treatment.

1. Introduction

Cancer treatment techniques are often associated with low efficiency and deleterious adverse effects. In general, it is attributed to poor penetration of anticancer drugs into malignant tumors. Therefore, high drug doses are usually administered to achieve efficient therapeutic outcome. However, prolonged application of cytostatic drugs causes detrimental secondary effects, (in-)directly leading to systemic organism intoxication and impairment of essential physiological functions. Classic anticancer drugs, such as bleomycin (BLM) or doxorubicin (DOX), induce toxic effects to multiple organ systems, including respiratory, cardiovascular, gastrointestinal, renal and reproductive. Prolonged

☆ This article is part of a special issue entitled: 'Power Ultrasound & Cavitation' published in Ultrasonics Sonochemistry.

* Corresponding author at: Research Institute of Natural and Technological Sciences, Vytautas Magnus University, Universiteto 10, Akademija, Kaunas District LT-53361, Lithuania.

E-mail addresses: martynas.maciulevicius@vdu.lt (M. Maciulevičius), lukas.giedrimas@vdu.lt (L. Giedrimas), ruta.palepsiene@ktu.lt (R. Palepšienė), paulius.ruzgys@vdu.lt (P. Ruzgys), rytis.jurkonis@ktu.lt (R. Jurkonis), mindaugas.tamosiunas@lu.lv (M. Tamošiūnas), renaldas.raisutis@ktu.lt (R. Raišutis), kristine.saleniece@lu.lv (K. Saleniece), saulius.satkauskas@vdu.lt (S. Šatkauskas).

https://doi.org/10.1016/j.ultsonch.2025.107381
Received 25 February 2025; Received in revised form 20 April 2025; Accepted 6 May 2025
Available online 8 May 2025

cancer treatment with BLM usually leads to severe lung diseases, while long-term use of DOX is usually associated with life-threatening heart failure [1,2]. Indeed, the study, which examined 600 death cases, that occurred during the first 30 days after the start of chemotherapeutic treatment, reported chemotherapy to be responsible for the premature death of 27 % patients [3]. Therefore, the development of less toxic anticancer agents and/ or treatment methods is highly required.

Sonoporation (SP) exploits ultrasound (US)- induced microbubble (MB) cavitation as the primary mechanism to facilitate bioactive compound delivery to cells and tissues [4]. Numerous relevant studies, which employed SP in combination with anticancer drugs, have demonstrated its therapeutic capacity to suppress or completely eradicate pancreatic [5], brain [6,7], ovarian [8,9], breast [10,11], prostate [12,13] and skin [14] cancer. Conventional chemotherapeutic drugs, such as BLM or DOX, are capable to induce cell death due to DNA intercalation. However, recent studies have focused on more fundamental, yet therapeutically potent agents, like calcium ions (Ca^{2+}). Indeed, Ca^{2+} plays an essential role in managing cellular response to diverse external triggers, including those directly related to cell mortality. A plethora of reseaerch has demonstrated that cell stimulation using external US field was capable to induce changes in Ca^{2+} content at the cellular level.

Pioneering studies have demonstrated that Ca^{2+} intracellular uptake can occur from the surrounding medium, even at physiological Ca^{2+} levels, following US-mediated MB activity [15,16]. These studies also determined that MB cavitation was responsible for Ca^{2+} delivery, since, only the cells, located in close vicinity to collapsing MBs, exhibited immediate Ca^{2+} influx. What is more, Ca^{2+} intake was simultaneously followed by propidium iodide (PI) influx and fura-2 dye loss, which can be considered as hallmarks of non-specific pore formation [15,16]. A direct relationship between cellular Ca^{2+} uptake and MB cavitation was also reported by Beekers et al. [17]. Their study showed that the profiles of Ca^{2+} influx were strongly correlated with the amplitude of MB oscillation. Furthermore, Ca^{2+} entry was closely associated with cell membrane permeabilisation and the opening of inter-cellular junctions. Study highlighted the contribution of cavitation to both intra-cellular signaling and tissue-level barrier disruption [17]. These studies have also reported propagation of Ca^{2+} waves, which originated from directly affected cells. Waves traveled at 7–20 μm/s speed towards the untreated cells, located in the periphery [15,17]. Such Ca^{2+} waves represent an additional mechanism of inter-cellular communication and a reliable option for therapeutic modulation beyond the immediate site of SP.

Additional Ca^{2+}-associated effects include: cytoskeleton rearrangement, delayed pore resealing and altered cell motility [18]. This broad-spectrum cellular response can persist from minutes to hours after US exposure, indicating a prolonged intra-cellular effect [18]. Furthermore, Memari et al. have reported cavitation-associated changes in intracellular Ca^{2+} levels, that were largerly dependent on MB behavior [19]. In particular, MB horizontal transit across the monolayer of endothelial cells, along with MB flow rate and a specific US pulsing pattern applied [19]. Collectively, these findings indicate that Ca^{2+} signaling is not a by-product of cell SP but rather a central mediator of biophysical responses to US-MB interaction. This mechanistic understanding of diverse Ca^{2+} roles in SP provides an important foundation for our study, which directly employs Ca^{2+} SP as a therapeutic strategy. We aim to achieve targeted cytotoxicity in cancer cells by modulating the level of intracellular Ca^{2+} via externally applied acoustic field.

Indeed, Ca^{2+} has a well-established history as a therapeutic agent in the field of cell electroporation (EP). Ca^{2+} EP has been validated to reduce cancer cell viability *in vitro* [20–22], induce tumor regression *in vivo* [20,21,23] and demonstrate promising outcomes in clinical trials involving human patients [24–28]. Notably, clinical studies have reported Ca^{2+} EP to induce comparable anticancer efficiency to conventional BLM-based electro-chemotherapy [24,25].

Elevated levels of intracellular Ca^{2+} are effectively disposed by intrinsic cell regulation mechanisms, developed to maintain homeostatic balance. Thus, in contrast to conventional chemotherapeutics, the employment of over-threshold Ca^{2+} doses offers a possibility to reduce harmful secondary effects. Indeed, recent clinical studies on Ca^{2+} EP have reported no or very little adverse effects, directly related to Ca^{2+} [24–28]. What is more, the adverse effects, attributed to Ca^{2+} EP have been reported to be lower than those, observed for conventional BLM-based electro-chemotherapy [26,28].

As a consequence, due to its efficiency, safety and symptom relief, Ca^{2+} EP has been integrated into clinical practice across Northern Europe for the treatment of (sub-)cutaneous metastases [26,27]. Current research also suggests that Ca^{2+} EP can significantly prolong the lives of patients, diagnosed with advanced stage pancreatic malignancies [29,30].

Our recent studies on Ca^{2+} SP have revealed that Ca^{2+} (<20 mM) could significantly reduce essential vital functions, directly associated to the survival of non-cancer Chinese hamster ovary (CHO) cells, including: i) membrane permeability, ii) metabolic activity, and iii) colony-formation efficiency. 5 mM concentration of Ca^{2+} was determined to be an efficient alternative to BLM (20 nM) for the efficient reduction of CHO cell viability [31,32]. Also, Ca^{2+}, being a diffusible secondary messenger, is crucial for the triggering of signal transduction pathways, (in-)directly associated with cell mortality. Due to large difference in Ca^{2+} levels across cell membrane, even a slight supra-physiological increment in Ca^{2+} concentration can rapidly initiate cell mortality. Indeed, Ca^{2+} SP caused the death of CHO cells within 15 min after US irradiation [31–33], which was faster compared to BLM SP [31,32] or Ca^{2+} EP [33].

Current study aims to evaluate the cytotoxic efficiency of Ca^{2+} SP across multiple experimental levels, including: i) 4 T1 cancer cells in a suspension, ii) 3-D cell spheroids and iii) subcutaneous tumors in murine models. To our knowledge, this is the first multi-level investigation of Ca^{2+} SP for cancer treatment. Parallel experimental series were conducted using BLM SP, enabling a direct and objective comparison between Ca^{2+}- and BLM-based therapeutic strategies. Additional biophysical insights into the mechanism of SP were provided through cavitation signal monitoring, US imaging of tumors and subsequent cavitation data analysis.

2. Materials & methods

2.1. SP of cells in a suspension

SP experiments on 4 T1 cell culture in a suspension were conducted using a custom-designed experimental chamber, comprising a bath, filled with degassed water (Fig. 1A) [34–38]. Electric signals were produced using the Picoscope 5242B signal generator (Picotech, UK) and subsequently amplified with a push–pull topology pulser (Kaunas University of Technology, Lithuania). US was produced by an unfocused 18 mm diameter transducer (Medelkom, Lithuania), with a center frequency of 1 MHz center frequency and a − 6 dB bandwidth range of 0.9–1.2 MHz. The hydrophone (HNR 1000, Onda Corp, USA) was used to calibrate peak negative acoustic pressure in the cuvette. All experiments were performed at room temperature (24 °C).

Murine breast cancer 4 T1 cells (CRL-2539) were acquired from the American Type Culture Collection (ATCC, Manassas, USA). Cells were cultured in RPMI medium, supplemented with 10 % of fetal bovine serum and 1 % of penicillin/ streptomycin solution. After trypsinization using trypsin-EDTA solution (Sigma-Aldrich, St. Louis, MO, USA), cells were suspended in a laboratory-made HEPES-based medium, containing 10 mM HEPES (Lonza, Basel, Switzerland), 250 mM sucrose (Sigma-Aldrich, St. Louis, USA), and 1 mM $MgCl_2$ (Sigma-Aldrich, St. Louis, MO, USA) [39–41]. 4 T1 cells (0.9×10^6 cells/ml) (in HEPES-based buffer) were administered with Sonovue MBs (Bracco diagnostics Inc, Switzerland) (2×10^7 MBs/ml) and 5 mM $CaCl_2$ (Lachema, Czech Republic) or 20 nM BLM (Teva, the Netherlands). The suspension was administered into experimental cuvette to the final 1 ml volume. MB

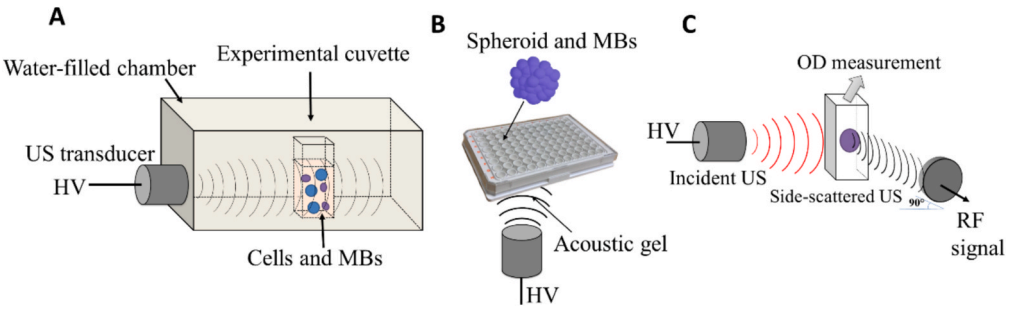

Fig. 1. Visual representation of US exposure setups, used for SP of cells in a suspension (A) and 3-D cell spheroids (B). Illustration of passive cavitation detection system, applied for the monitoring of MB cavitation at *in vitro* conditions (C). Abbreviations: HV – high voltage; RF – radio-frequency; OD – optical density.

concentration measurements were performed using spectroscopic method, previously developed by our group [38].

Experimental groups, involving Ca^{2+} or BLM, in combination with US alone or with SP, are presented in Table 1.

Cell SP was conducted using 1 MHz central frequency pulsed US, with 100 μs ON and 900 μs OFF durations, resulting in 10 % duty cycle. US pulses were delivered at 1 kHz pulse repetition frequency. For cell suspension experiments, US peak negative acoustic pressure ranged from 0 to 200 kPa, with a total exposure duration of 6 s.

Following US exposure, the cell suspension was incubated for 10 min at 37 °C in 5 % CO_2 atmosphere. Then, the cells were resuspended in growth medium for viability assessment using the following tests: i) PI assay (after 15 min), ii) MTT assay (after 48 h) and iii) cell clonogenic assay (CA) (after 6 days). The procedures are extensively described in our previous works [31–33].

2.2. SP of 3-D cell culture

Spheroids were cultivated in 96-well microplate (polystyrene, uncoated) (Celltreat, Pepperell, USA), coated with 1.5 % agarose. One well contained 100 μl of 0.02 mln/ml cells. Spheroids were grown for 5–6 days; growth medium was changed every day. After incubation period, spheroids were morphologically evaluated and selected for further use in the research.

Experiments were performed in 96-well microplate. Each well contained 200 μl volume of experimental buffer, containing MBs (2×10^7 MBs/ml) and/or 5 mM Ca^{2+}. Control group was supplemented only with experimental buffer. Experimental groups are presented in Table 2. Previously specified US transducer (Medelkom, Lithuania) was attached to the bottom of 96-well microplate using acoustic transmission gel (Rich Mar, Inola, USA) (Fig. 1B). Acoustic pressure in the well was calibrated using hydrophone (HNR 1000, Onda Corp, USA). Applied US parameters were the same as for cell suspension. Spheroids were grown for 6 days at 37 °C in 5 % CO_2. Their size (area) was evaluated by taking photographs every 1–2 days.

Table 1
Description of the experimental groups for SP in cell suspension.

Group	Ca^{2+}	BLM	MBs	US
Control	–	–	–	–
Ca^{2+} alone	+	–	–	–
BLM alone	–	+	–	–
US alone	–	–	–	+
Ca^{2+} + US	+	–	–	+
BLM + US	–	+	–	+
SP	–	–	+	+
Ca^{2+} SP	+	–	+	+
BLM SP	–	+	+	+

Table 2
Description of the experimental groups for SP of 3-D cell culture.

Group	Ca^{2+}	MBs	US
Control	–	–	–
Ca^{2+} alone	+	–	–
US alone	–	–	+
Ca^{2+} + US	+	–	+
SP	–	+	+
Ca^{2+} SP	+	+	+

2.3. SP of subcutaneous tumors

All animal procedures were performed in accordance to national and international guidelines on the use of laboratory animals. The study protocol was approved by Lithuanian State Food and Veterinary Service (Permit No. G2-149, issued on 2020–05-05). *In vivo* experiments adhered to international ARRIVE guidelines.

Eight- to twelve-week-old female BALB/c mice (Vilnius, Lithuania) were used in the research. Mice were housed under standard laboratory conditions, monitored 2–3 times daily for clinical signs of pain, distress or other abnormal behavior. All procedures, including sedation, anticancer agent administration and US exposure were conducted by trained personnel (license No. PK 46564) in accordance with the principles of Good Laboratory Practice (GLP). No significant adverse effects or welfare concerns were observed throughout the study. Animals maintained normal physiological and behavioral functions until euthanasia.

For tumor formation, 100 μl of 4 T1 cell suspension (20×10^6 cells/ml) was injected into the subcutaneous layer on dorsal caudal side of the mouse. Tumors reached sufficient experimental size at 9–12 days after the injection. Mice were randomly divided into experimental groups (10 mice per group) as indicated in Table 3. When the size of tumors exceeded 2 cm^3, mice were euthanized by CO_2 inhalation under the guidelines of GLP.

SP experiments were performed after mice were injected with sedatives, mixture of ketamine and xylazine, at a ratio of 87.5 and 12.5 mg/kg, respectively. For Ca^{2+} SP, 100 μl volume of $CaCl_2$ solution (150 mM) in 0.9 % saline was administered via intra-tumoral injection. For BLM SP, a solution containing 100 μl of BLM, diluted in saline at a concentration of 450 μM, was administered via injection into the tail vein. Mice were administered with intratumoral injection of 100 μl Sonovue MBs

Table 3
Description of the experimental groups for tumor treatment.

Group	Ca^{2+}	BLM	MBs	US
Control	–	–	–	–
Ca^{2+} alone	+	–	–	–
BLM alone	–	+	–	–
SP	–	–	+	+
Ca^{2+} SP	+	–	+	+
BLM SP	–	+	+	+

(3×10^8 MBs/ml), prepared in 0.9 % NaCl. After 3–4 min tumors were treated with continuous wave (CW) ~ 0.95 MHz center frequency 2 W/cm^2 intensity US for 60 s. US was produced by sonoporator (Sonitron 2000, RichMar, Inola, USA) using 18 mm diameter 1 MHz center frequency US transducer. Sonitron device was adjusted to 1 MHz center frequency, however, real US center frequency was evaluated to be ~ 0.95 MHz (Fig. 7B) using passive cavitation detection system.

In experimental groups, devoid of Ca^{2+}, BLM or MBs, mice were administered with equal volume of NaCl solution. After tumor treatment with SP, there was no significant change in temperature of the tumor (<1 °C). Tumor growth measurements were documented regularly (every 2 days) by Vernier caliper in two dimensions. The length (a) and the width (b) of the tumor were evaluated [42]. Tumor volume (V) was calculated as [43]:

$$V = ab^2/2 \quad (2.\ 3.\ 1)$$

The experimental data-points, representing tumor volume decrease against days after treatment, were approximated with exponential function [44]. Exponential function rate (α) was used to quantify tumor volume (V) reduction:

$$V(t) = Ae^{-\alpha t} + B \quad (2.\ 3.\ 2)$$

A – exponential function amplitude; B – offset; t – duration, α – tumor volume reduction rate.

2.4. Cavitation dynamics monitoring

2.4.1. Side-scattering signal Acquisition and analysis

Signal Acquisition *in Vitro*. MB side-scattered US waves were registered using passively-coupled 8 mm diameter US transducer (5 MHz center frequency, 2.1–7.9 MHz bandwidth at − 6 dB) (Doppler Electronic Technologies, Guang Zhou, China), positioned at 90° angle relative to the excitation transducer (Fig. 1C). The signals were recorded using oscilloscope (Picoscope 5242B, Picotech, UK) with a sampling rate of 31.25 MS/s and 8-bit resolution. Frame rate was 16.7 frames/s, frame duration – 10 ms.

Signal Acquisition *in Vivo*. Side-scattered US waves were registered using the same US transducer (Doppler Electronic Technologies, China), positioned at 90° angle relative to the transmitter and attached directly to the tumor. Acoustic transmission gel was used to maintain acoustic contact. US signals were acquired at a sampling rate of 17.86 MS/s with 8-bit resolution. During the 60 s total exposure duration, 920 frames were recorded, corresponding to frame rate of 15.3 frames/s, each frame of 2 ms duration.

Signal Analysis. The procedure for radio-frequency signal processing is similar as described in detail in our previous articles [34–37,44]. Fast Fourier transform (FFT) was used to create frequency spectrum of registered US waves. FFT amplitude values are reported in decibels relative to 1 V (dBV), indicating that the measurements are referenced against a 1 V baseline. Subsequently, root mean square (RMS) values were calculated in a specific frequency range (equation 2. 4. 1. 1):

$$RMS(t) = \sqrt{\frac{1}{n}\left(x_1^2 + x_2^2 + \cdots + x_n^2\right)} \quad (2.\ 4.\ 1.\ 1)$$

where n – total number of values in FFT spectrum, x – amplitude value.

For *in vitro* experiments, the influence of systemic US background was diminished by subtracting RMS, obtained without the administration of MBs. For *in vivo* data, the average of constant RMS data-points, obtained before RMS increase and/or after RMS decrease (corresponding to background RMS), was subtracted from the original curve. Cavitation dose (CD), was quantified as the integral of the RMS curve, plotted against exposure duration [45]:

$$CD = \int_{0s}^{60s} RMS(t)dt \quad (2.\ 4.\ 1.\ 2)$$

where t – time, *0 s* – the onset of US exposure, *60 s* – the end of US exposure.

2.5. US imaging

Tumor imaging was performed using diagnostic US system (MentorTM, Advent, USA). Personal computer was upgraded with video input adapter (AVerTV USB2.0 Plus, AVerMedia Technologies Inc., Taiwan) to record sequences of B-scan images for the off-line analysis. A large amount of acoustic transmission gel was used to form a layer of more than 5 mm between the imaging transducer and the skin of mouse. Central frequency of diagnostic US transducer was 15 MHz. B-scan images were recorded at frame rate of 30 frames/s, imaging depth was up to 35 mm. Mean pixel intensity was calculated in a circular region of interest (ROI). The resultant values were plotted against exposure duration and approximated with Boltzmann sigmoidal function [36]:

$$Intensity(t) = \frac{A_1 - A_2}{1 + e^{k(t-t_c)}} + A_2 \quad (2.\ 4.\ 2.\ 1)$$

where *A1* – initial intensity value, *A2* – final intensity value, k –rate constant; t – time; t_C – time at the center of sigmoidal curve.

2.6. Data analysis

Results for *in vitro* experiments are reported as mean ± standard error (SEM) of mean of at least 3 independent experiments (in total at least 6 replicates); for *in vivo* experiments – of 10 animals (or tumors) per group. Statistical significance was evaluated using Mann-Whitney test. US signals and images were analyzed using Matlab (Mathworks, USA). Data analysis was performed using Origin (OriginLab Co, USA) software.

3. Results

3.1. Ca^{2+} and BLM Sonotranfer into 4 T1 cells in a suspension

The results for Ca^{2+} (5 mM) or BLM (20 nM) sonotransfer into 4 T1 cancer cells in a suspension are presented in Fig. 2 (A1-D1 for Ca^{2+} SP and A2-D2 for BLM SP).

Obtained data indicates that Ca^{2+} in tandem with US exposure significantly reduce cell viability. 4 T1 cells progressively die during the duration up to 6 days – cell death occurs earlier, if exposed to higher acoustic pressure (Fig. 2B1). On the contrary, the combination of BLM and US fails to induce higher cell death – in the range of acoustic pressure up to 200 kPa, cell viability sustains above ~ 80 % (Fig. 2B2).

The addition of MBs significantly enhanced cell mortality, induced by Ca^{2+} (Fig. 2C1) – after 6 days only 50 % of cells were viable at 50 kPa and only 10 % – at 200 kPa. Similarly, the cytotoxicity of BLM was enhanced by the administration of US contrast agents. However, more pronounced effect was observed only at 200 kPa (Fig. 2C2). The comparison of data, given in Fig. 2C1 and 1C2 indicates that Ca^{2+} requires lower acoustic pressure to induce efficient cell death. Furthermore, Ca^{2+} acts faster – at 100 kPa only 50 % of cells are viable (Fig. 2C1), whereas for BLM – the viability is ~ 90 % (Fig. 2C2). Indeed, the administration of MBs significantly enhanced cell mortality at 100 kPa (Fig. 2D1), whereas for BLM – only at 200 kPa. Also, Fig. 2D2 demonstrates that the highest decrease in cell viability for the combination of BLM + MB + US occurred only after 48 h, whereas for Ca^{2+} – it was observed after 15 min (Fig. 2D1). In addition, Ca^{2+} at 100–200 kPa US acoustic pressure (Fig. 2D1) reduced cell viability to ~ 25–30 % without the administration of MBs, whereas effective performance of BLM required the presence of MBs (Fig. 2D2).

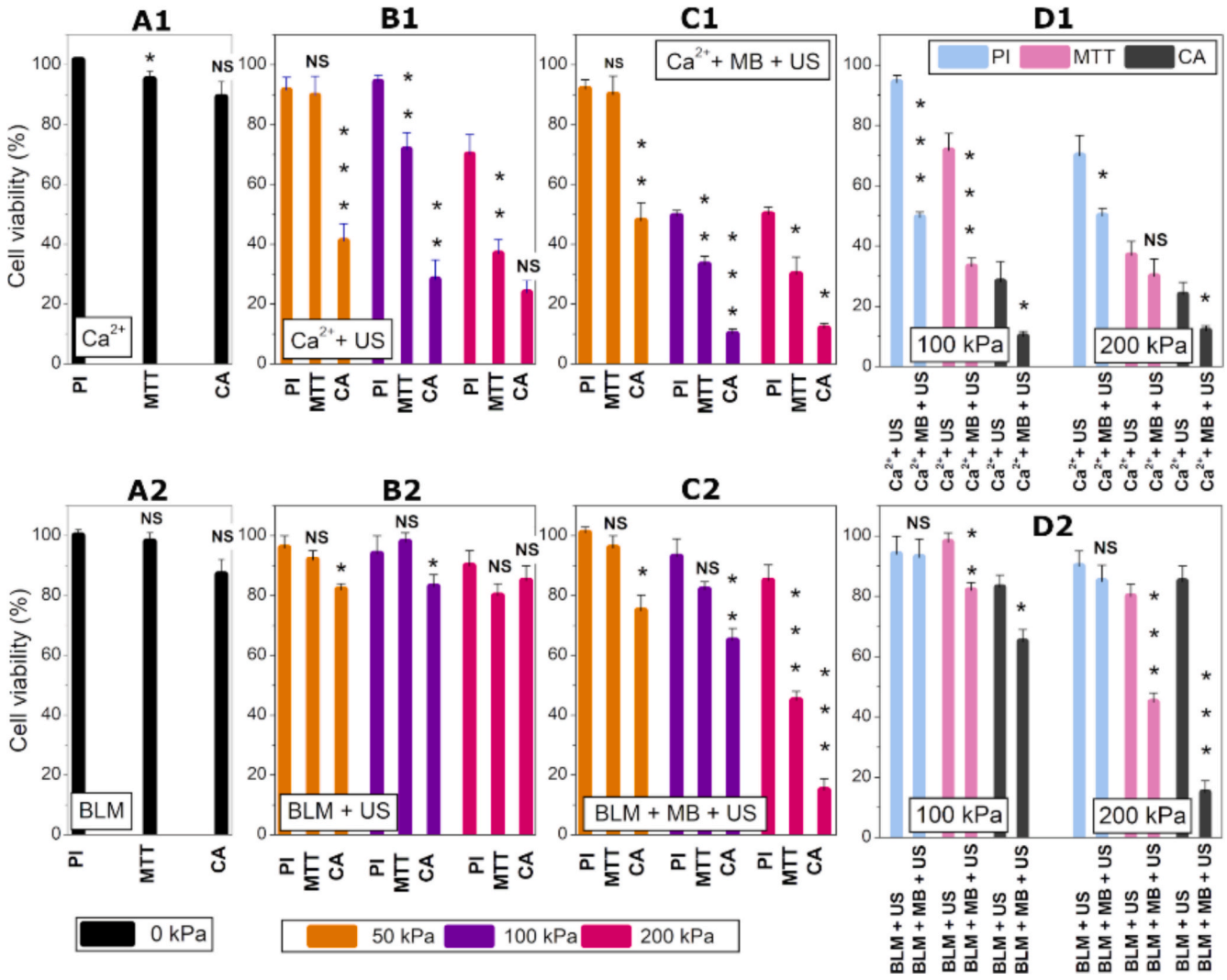

Fig. 2. Ca^{2+} and BLM sonotransfer into 4 T1 cells in a suspension. Cell viability was evaluated after 15 min (PI assay), 48 h (MTT assay) and 6 days (CA). Cell viability for Ca^{2+} alone (0 kPa) (A1); Ca^{2+} + US (B1) and Ca^{2+} + MB + US (C1) at 50–200 kPa acoustic pressure; cell viability data for Ca^{2+} + US and Ca^{2+} + MB + US, grouped according to acoustic pressure (D1). Cell viability for BLM alone (0 kPa) (A2); BLM + US (B2) and BLM + MB + US (C2) at 50–200 kPa acoustic pressure; cell viability data for BLM + US and BLM + MB + US, grouped according to acoustic pressure (D2). "NS" – not significant; * – $p < 0.05$; ** – $p < 0.01$; *** – $p < 0.001$.

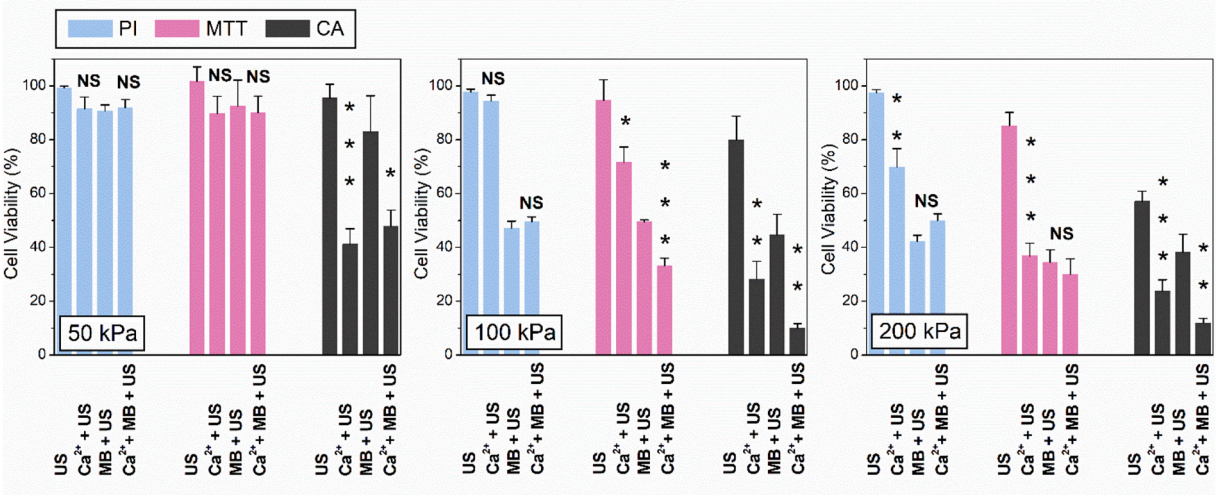

Fig. 3. 4 T1 cell viability for US, Ca^{2+} + US, MB + US and Ca^{2+} + MB + US at 50–200 kPa acoustic pressure. Cell viability was evaluated after 15 min (PI assay), 48 h (MTT assay) and 6 days (CA). "NS" – not significant; * – $p < 0.05$; ** – $p < 0.01$; *** – $p < 0.001$.

Secondly, we have quantified the proportion of cells, which died due to i) MB cavitation and ii) Ca^{2+} delivery. Therefore, we have compared the percentage in cell mortality between Ca^{2+} + US and US groups as well as between Ca^{2+} + MB + US and MB + US groups (Fig. 3).

Results indicate that Ca^{2+} induces pronounced cytotoxicity already at 50 kPa even in the absence of MBs. This is indicated by a high difference in cell mortality, observed for US and Ca^{2+} + US after 6 days (CA). The increase in acoustic pressure up to 100 kPa resulted in a relevant cell mortality increase, observed after 48 h (MTT test). Whereas, additional pressure increase (up to 200 kPa) resulted in significant cell death, observed even after 15 min (PI test). The highest differences in cell viability between Ca^{2+} + US and US experimental groups were observed for 50 and 100 kPa (CA, 6 days) as well as 200 kPa acoustic pressure (MTT, 48 h).

In overall, up to 50 % of cell population died due to Ca^{2+} intracellular sonotransfer. The proportion of cavitation-induced cell death was high in the groups, administered with MBs, therefore, cell death due to Ca^{2+} was estimated to be lower.

3.2. Ca^{2+} Sonotranfer into 3-D cell cultures

After successful validation of Ca^{2+} SP in cell suspension, we have transitioned to 3-D culture (Fig. 3). Cytotoxic effect of Ca^{2+} for cell spheroids was evaluated using 400 (Fig. 4B) and 700 (Fig. 4B) kPa acoustic pressure.

Ca^{2+} or Ca^{2+} + US were only able to sustain spheroid size around its initial level (Fig. 4B and C). The application of US at 400 or 700 kPa acoustic pressure was not effective in reducing spheroid growth either. However, cavitation at 700 kPa acoustic pressure was capable to inhibit the growth of 3-D cell cultures up to the ~ 4th day. The only treatment, which significantly down-sized the spheroid volume was the application of Ca^{2+} combined with MB cavitation at 700 kPa acoustic pressure. Fig. 4D visually illustrates the dynamics of spheroid growth. In both control and Ca^{2+} groups the size of spheroids increased throughout the whole 6-day period. The application of Ca^{2+} + US (at 700 kPa acoustic pressure) slightly reduced the growth of spheroids. Not surprisingly, the highest changes in spheroid morphology were observed for cavitation (MB + US) as well as therapeutic (Ca^{2+} + MB + US at 700 kPa) groups. Cavitation resulted in spheroid tearing, however, the remaining pieces of a spheroid eventually increased in size. In the therapeutic group, cavitation also induced spheroid disintegration, however, the remaining cell clusters did not exhibit the tendency to grow. This effect was attributed to Ca^{2+}. Conversely to cells in a suspension, the significant cytotoxic effect of Ca^{2+} for spheroids required the administration of MBs as well as higher acoustic pressure, however, was achieved at pulsed US mode.

3.3. Cavitation dynamics for in vitro experiments

To gain insight into the biophysical mechanisms, underlying biological cell and spheroid response, we have performed the analysis MB side-scattered US waves and MB concentration measurements (Fig. 5). Representative side-scattering US pulses and their corresponding time–frequency-amplitude colormaps are presented in Fig. 5A and B, respectively.

The data indicates that at low acoustic pressure of 100 kPa, MB cavitation signal is weaker and persists for a longer duration compared to 200 kPa. At 200 kPa acoustic pressure, stronger cavitation emissions were observed in a broad frequency range, lasting for up to 4 s (Fig. 5B). The colormap, presented for – MB group at 200 kPa, represents the spectral characteristics for US alone – with no broad-band noise occurring. Correspondingly, increased efficiency in Ca^{2+} and BLM sonotransfer was determined to be higher at 200 kPa, compared to 50 and 100 kPa acoustic pressures.

Higher 250 and 300 kPa acoustic pressures indicated shorter acoustic emissions lasting for ~ 3 s and ~ 2 s. respectively. High acoustic pressures of 400 and 700 kPa were determined to have strong but short-lived cavitation charasteristics – lasting for > 1 s for 400 kPa and < 1 s for 700 kPa.

In our previous research on MB cavitation, we have shown that cavitation dynamics of Sonovue MBs could be well-characterised, if RMS was quantified in 1.5–1.75 MHz frequency range [34–37,44]. Similar calculation of RMS has revealed different curve patterns for low (50 and 100 kpa) (Fig. 5C), intermediate (200 and 300 kPa) (Fig. 5D and E) and

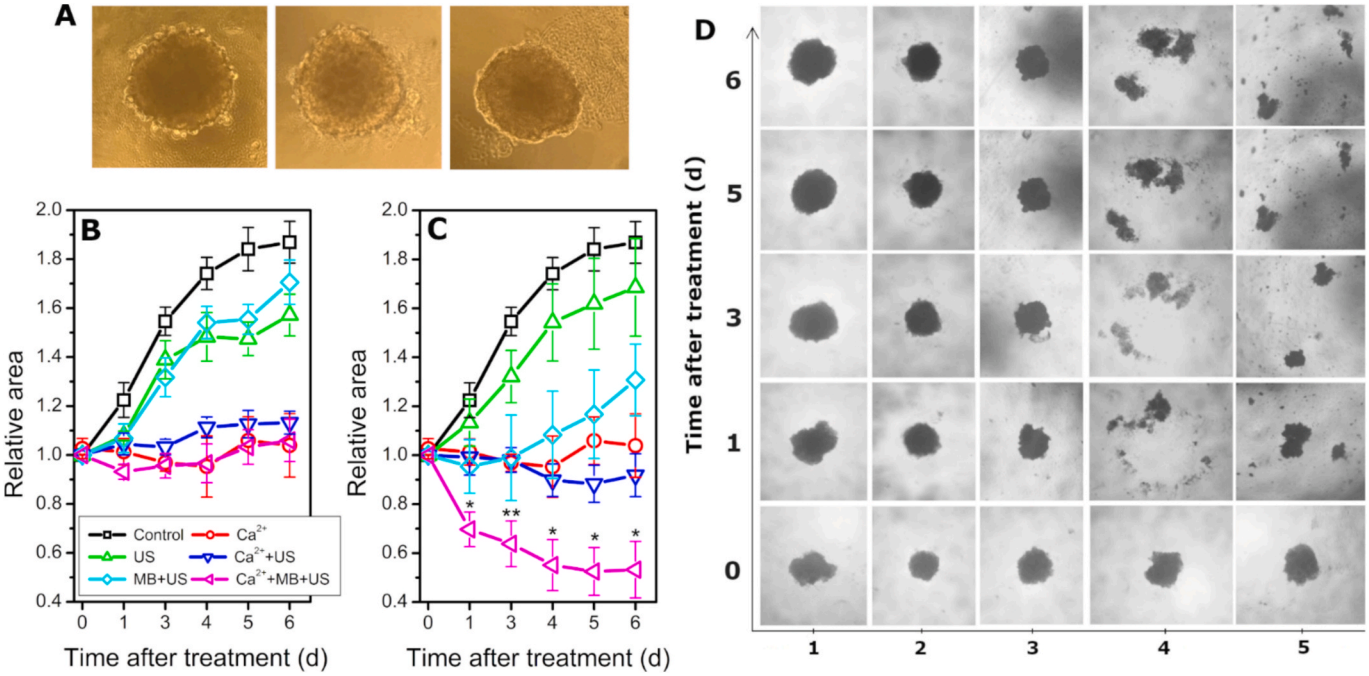

Fig. 4. Ca^{2+} sonotransfer to 3-D culture of 4 T1 cells. 4 T1 cell spheroids in agarose gel (A). The results of spheroid growth for different experimental groups at 400 (B) and 700 (C) kPa acoustic pressure. Microscopical images of spheroids: 1- control; 2- Ca^{2+}; 3- Ca^{2+} + US (700 kPa); 4- MB + US (700 kPa); 5- Ca^{2+} + MB + US (700 kPa). "NS" – non-significant; * – $p < 0.05$; ** – $p < 0.01$; *** – $p < 0.001$.

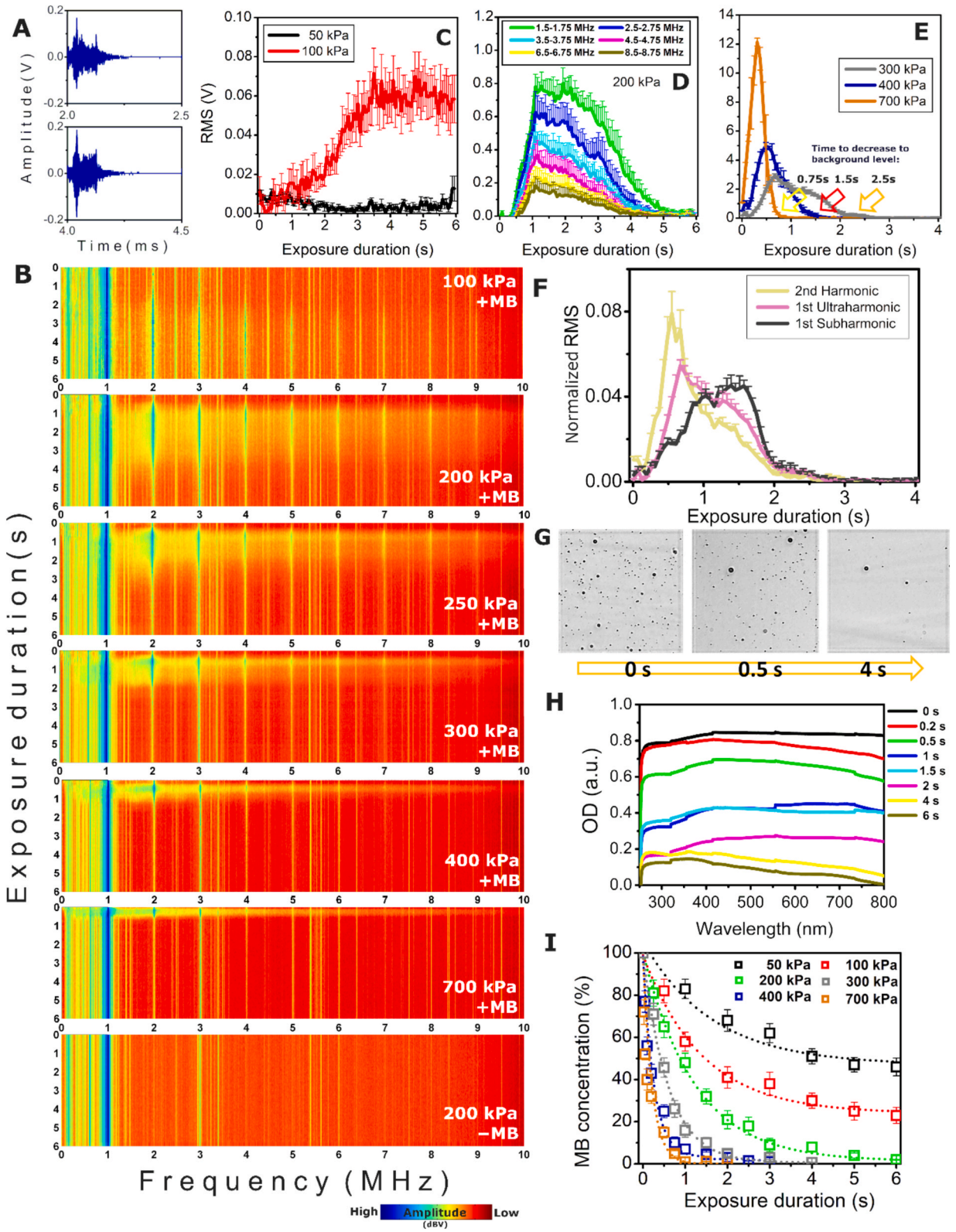

Fig. 5. The dynamics of US side-scattered signals and MB concentration. Representative side-scattered US pulses (A). Processed, filtered (4th order Butterworth filter) and averaged (n = 4 different experiments) time–frequency-amplitude colormaps: i) for MB-containing (+MB) groups at 100–700 kPa; ii) MB-free (−MB) group for 200 kPa (B). RMS curves, quantified in 1.5–1.75 MHz frequency range, for low 50 and 100 kPa acoustic pressures (C). RMS dynamics, evaluated across different frequency ranges, for 200 kPa acoustic pressure (D). RMS curves, quantified in 1.5–1.75 MHz frequency range, for 300, 400 and 700 kPa acoustic pressures (E). Normalised RMS curves for 300 kPa, quantified in frequency range of ± 0.1 MHz around: the 2nd harmonic *(2f)*, 1st ultraharmonic *(3/2f)* and 1st subharmonic *(1/2f)*; $f = 1$ *MHz* (F). Micrographs, illustrating MB concentration decrease, at 200 kPa acoustic pressure (G) and corresponding OD values, representing MB concentration decrease (H). Temporal MB concentration decrease for 50–700 kPa acoustic pressures (I).

high (400 and 700 kPa) (Fig. 5E) acoustic pressures. At the level of 50 kPa, RMS did not display a notable increase, whereas, at 100 kPa, RMS started to increase from ~ 1 s (Fig. 5C). For the acoustic pressure of 200 kPa, RMS curves, quantified in higher frequencies, had significantly lower values compared to 1.5–1.75 MHz (Fig. 5D). This tendency goes in line with the findings observed in time–frequency-amplitude colormap for 200 kPa. Additionally, the width of RMS curve exhibited a decreasing trend with increasing frequency (Fig. 5D). Indeed, RMS curve, quantified in 1.5–1.75 MHz frequency range, reached background level of 0 V at approximately 5 s. At high acoustic pressures, 400 and 700 kPa, MB cavitation activity was much more transient with RMS curves persisting for ~ 1.5 s and ~ 0.75 s, respectively. Consequently, efficient spheroid shrinkage was achieved only for therapeutic Ca^{2+} + MB + US group at 700 kPa, suggesting that short, yet highly energetic, MB inertial cavitation is a requisite for the efficient therapeutic outcome for cell spheroids.

In the beginning of US exposure, RMS, calculated for the 2nd harmonic showed the fastest increase, subsequently followed by ultraharmonical RMS (Fig. 5F). Interestingly, subharmonical RMS was increasing significantly slower than other curves and, therefore, sustained relatively high for the longest period of time. Consequently, harmonical RMS rapidly decreased, while RMS, evaluated in subharmonical range, sustained. Ultraharmonical RMS indicates a transition between other two RMS curves. Fast decrease of harmonical RMS, accompanied by delayed ultraharmonical and, especially, prolonged subharmonical RMS, indicate energy transition from frequency components, associated to linear MB behavior, to more non-linear, that is followed by MB collpase (Fig. 5I).

The decrease in MB concentration was examined by monitoring optical density (OD) values [38]. Representative micrographs, indicating the decrease in MB concentration, and corresponding OD values for 200 kPa acoustic pressure are given in Fig. 5G and H, respectively. The obtained MB concentration dynamics across different acoustic pressures indicate slow MB sonodestruction at low acoustic pressures (50 and 100 kPa) compared to high (400 and 700 kPa). Similarly to RMS trends, observed at 1.5–1.75 MHz frequency range, MB sonodestruction was longer than 6 s for 50 and 100 kPa acoustic pressures, whereas for 200 kPa it lasted for ~ 6 s. In contrast, MB sonodestruction was significantly faster for 400 and 700 kPa acoustic pressures, occurring within ~ 2 s and ~ 1 s, respectively.

Altogether, these findings indicate that high acoustic pressures resulting in rapid MB sonodestruction and pronounced MB cavitation activity are essential to achieve required therapeutic effect for 3-D cell culture. On the contrary, cells in a suspension well-responded to longer, yet not so intense, MB cavitation activity.

3.4. Ca^{2+} and BLM Sonotranfer into tumors

Eventually, we have evaluated the therapeutic effect of Ca^{2+} SP for 4 T1 subcutaneous tumors in BALB/c mice (Fig. 6). In this case, only Ca^{2+} SP and BLM SP were able to completely eradicate the tumors. A significant decrease in tumor volume was observed from the third day after treatment (Fig. 6B).

The evaluated decrease rate of 4 T1 tumors was similar for both therapeutic approaches, Ca^{2+} SP as well as BLM SP. This implies that Ca^{2+} is a valid anticancer agent, competitive with BLM (Fig. 6C insert). Therefore, in the long-term, it could be used as a promising alternative, if combinated with SP. Furthermore, all mice were successfully healed in both Ca^{2+} SP and BLM SP groups. However, three mice died after the treatment in BLM + SP group and one mouse in Ca^{2+} SP group, as

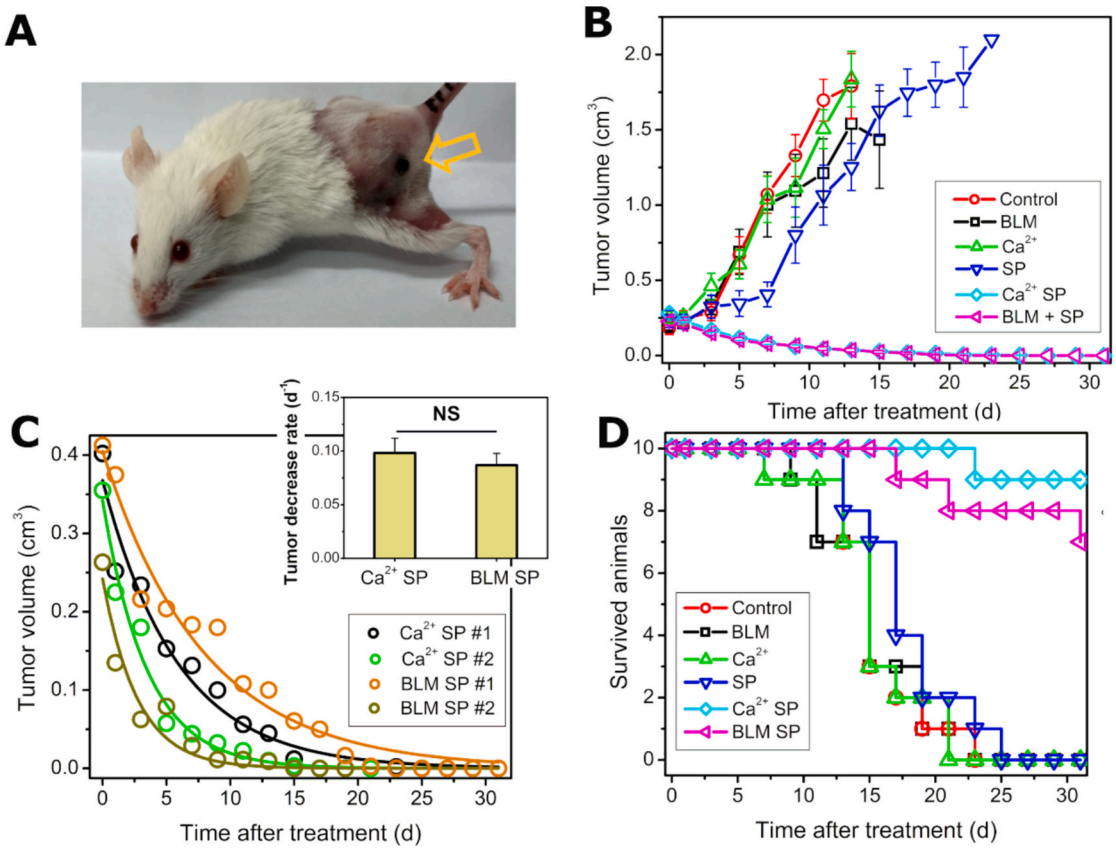

Fig. 6. Ca^{2+} and BLM sonotransfer into subcutaneous tumors of 4 T1 breast cancer cells. Mouse image, representing the site of healed tumor (yellow arrow) after Ca^{2+} SP (A). The dynamics of tumor volume during post-treatment period (B). Quantification of tumor volume reduction rate using exponential curve fitting (C); tumor reduction rate for Ca^{2+} SP and BLM SP (C inset). Mouse survivability, illustrated by Kaplan-Meyer curves for each experimental group (D).

indicated by Kaplan-Meyer curves in Fig. 6D.

3.5. Cavitation dynamics for in vivo experiments

3.5.1. US side-scattering data

The setup, used for *in vivo* experiments is illustrated in Fig. 7A. US side-scattering signals were acquired during tumor SP, the obtained signal spectral content is presented in Fig. 7B. FFT spectra indicate the highest cavitation activity, occurring in 1–4 MHz frequency range. This tendency is consistent with *in vitro* cavitation dynamics, previously presented in Fig. 5B.

Similarly to *in vitro* analysis, we have selected 1.5–1.75 MHz frequency band for the quantification of RMS values. This frequency range exhibited a notable difference in FFT amplitudes between MB-containg (MB + US) and MB-free (US alone) groups (Fig. 7B inset). Interestingly, this frequency range has been reported to efficiently characterise MB cavitation activities in our previous *in vivo* research [44]. When plotted against exposure duration, RMS curve, quantified for + MB group, displayed a distinct phase of gradual increase, followed by a subsequent decrease. Whereas RMS, obtained for − MB group, resulted in a steady curve, representing a noise-dominated baseline (Fig. 7C).

The incremental dynamics of FFT spectra are demonstrated Fig. 7D. The frequency components within 1.5–1.75 MHz range are progressively increasing, as the time frames approach the maximal values of RMS curve. The spectra, presented in Fig. 7D, correspond to data-points, present in the red curve (MB + US #2), which is shown in Fig. 7F and I. The highest FFT amplitudes are observed in the 164th frame (10.6 s), coinciding with the highest RMS value in the red curve. Additionally, Fig. 7D demonstrates that RMS values decrease significantly, as the frequency ranges are selected beyond 1.5–1.75 MHz. The highest RMS curves in 1.5–1.75 MHz frequency range may be associated to Sonovue MB resonant frequency, determined to fall within 1.5–1.8 MHz frequency range [46,47]. Thus, in this region MB cavitation activity might be expected to be the highest and the most informative.

The same FFT spectra are represented at increasing temporal order in Fig. 7E. Both FFT spectra (Fig. 7E) and harmonical RMS values (Fig. 7G)

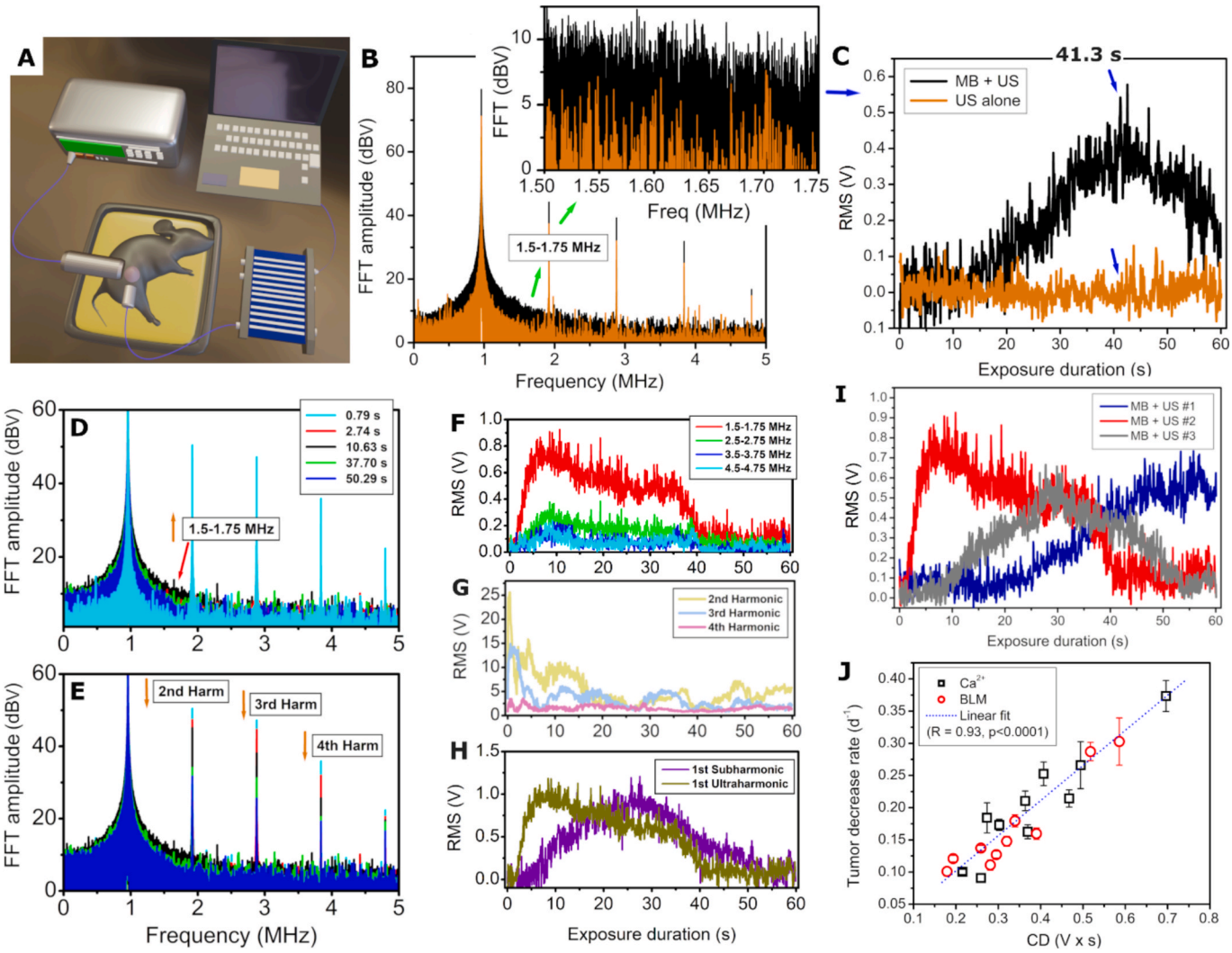

Fig. 7. Schematic representation of US-side scattered signal registration (A). Frequency spectra for MB-containing (MB + US) and MB-free (US alone) groups (B), shown for the frame #634 (41.3 s); the inset highlights frequency spectra within 1.5–1.75 MHz frequency range. RMS curves for + MB and − MB groups, quantified in 1.5–1.75 MHz frequency range (C); frame #634 is indicated by blue arrows. Temporal increase in FFT amplitude in 1.5–1.75 MHz frequency range (D). Temporal decrease in FFT amplitude for the 2nd *(2f)*, 3rd *(3f)* and 4th *(4f)* harmonics *(f = 0.95 MHz)* (E). RMS curves, evaluated in 1.5–1.75 MHz frequency range and its corresponding repetitive ranges at higher frequencies (F). RMS curves, quantified within ± 0.1 MHz frequency band around the 2nd *(2f)*, 3rd *(3f)* and 4th *(4f)* harmonics (G). RMS curves, calculated within ± 0.1 MHz frequency band around the 1st suharmonic *(1/2f)* and 1st ultraharmonic *(3/2f)* (H). Examples of the variability in RMS curves (1.5–1.75 MHz), obtained from different tumor samples (I). The correlation between CD and tumor decrease rate, pooled for Ca^{2+} SP and BLM SP (J).

show a decreasing trend over time. The latter tendency suggests an energy shift (quantified in RMS) from harmonic frequencies to sub-harmonic and ultraharmonic (Fig. 7H) as well as interharmonic frequency components (Fig. 7F).

Fig. 7I demonstrates the variability in obtained RMS curves for different tumors within therapeutic group. While all the curves have clearly defined phases of increment, peak and decrement, the variations in shape and amplitude are observed among individual tumors. These differences can be attributed to different tumor size/ shape, heterogeneity of cancer tissue as well as varied distribution of MB bolus within the tumor.

Eventually, integral CD values were quantified using RMS curves. A strong ($R = 0.93$) and statistically significant ($p < 0.0001$) correlation was determined between CD and tumor decrease rate (Fig. 7J). Data suggest that Ca^{2+} SP or BLM SP can efficiently induce the regression of 4 T1 tumors in mice even at low CD, without pronounced lethal effects of inertial cavitation, as the absolute majority of animals survived the treatment.

3.5.2. *Tumor imaging data*

Internal distribution of MBs within the tumor was monitored using B-scan imaging technique (Fig. 8). Gradual decrease of MB back-scattering intensity, evaluated in the ROI area, is displayed in chronological order (0–60 s) (Fig. 8A). MB shadow is visible on the right to ROI area (yellow arrow). The disappearance of the shadow region occurs simultaneously with a decrease in back-scattering intensity at the location of MB bolus.

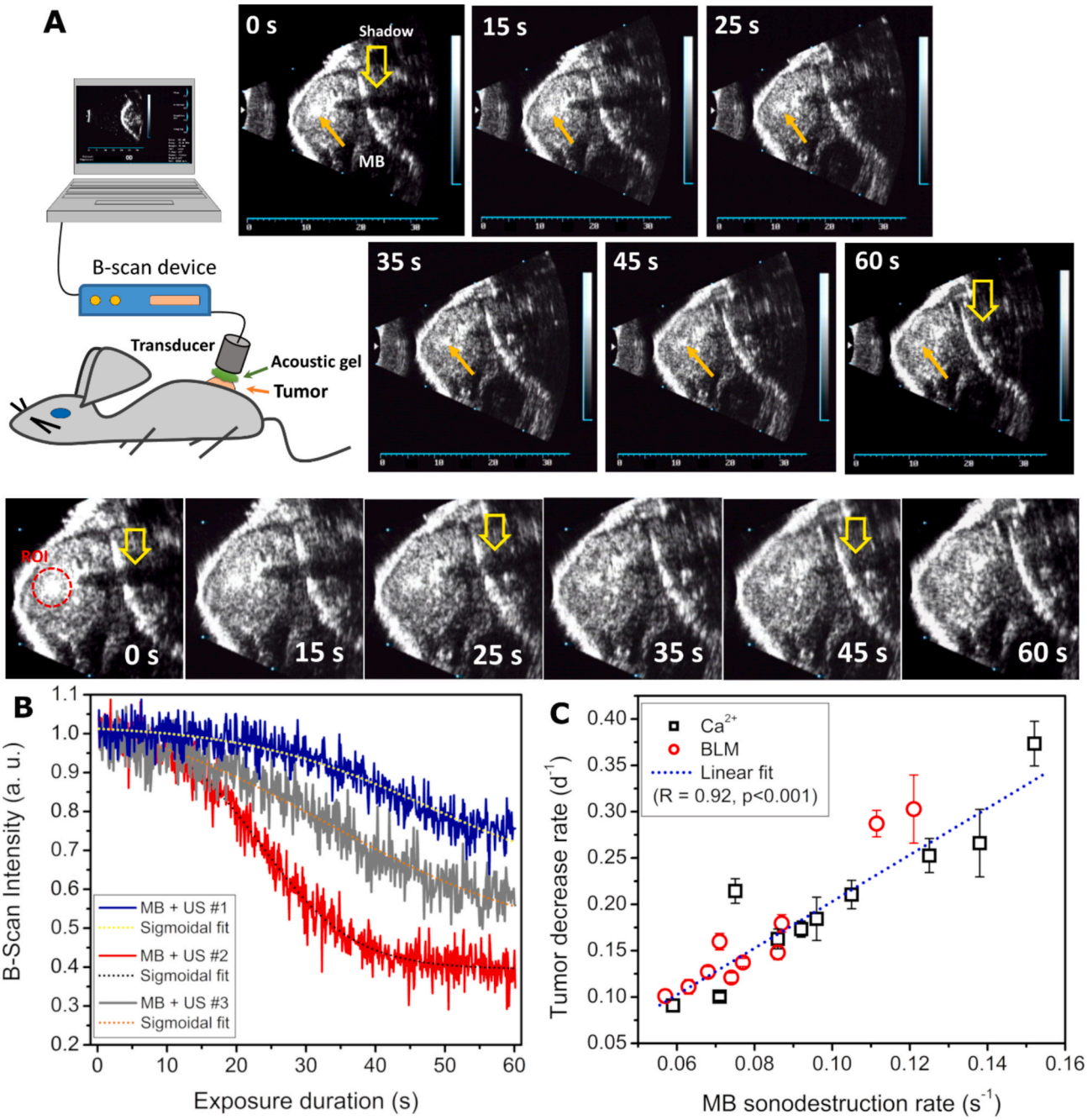

Fig. 8. US diagnostic imaging of subcutaneous tumors. A gradual reduction in the intensity of US back-scattered signal in MB bolus (orange arrow in upper panel) or ROI (red circle in lower panel) areas, followed by simultaneous disappearing of MB shadow (yellow arrow) (A). Normalised B-scan intensity curves with respective sigmoidal approximations, obtained from different tumors (B). The correlation between MB sonodestruction rate and tumor decrease rate (C).

The obtained back-scattering curves were plotted against exposure duration and approximated with a sigmoidal function, as demonstrated in Fig. 8B. Subsequently, tumor decrease rate was plotted in dependence on MB sonodestruction rate (Fig. 8C). Strong ($R = 0.92$) and significant ($p < 0.001$) correlation between MB sonodestruction rate and tumor decrease rate were obtained for the data of Ca^{2+} SP and BLM SP.

In general, both correlation assays indicate that higher tumor decrease rate is associated with higher MB cavitation acitivity, that can be directly associated with faster MB sonodestruction. Since the absolute majority of mice were healed, the exposure of animals to SP conditions, associated with lower CD or MB sonodestruction rate, was more favorable. This was because mice achieved less negative impact of US/cavitation and were still successfully healed.

3.5.3. CD and MB sonodestruction rate correlation

In previous studies, we have determined strong correlation between CD and MB sonodestruction rate for *in vitro* conditions [34,36]. Currently, we were able to broaden our previous approach and introduce robustness for the observed phenomenon by achieving similar result at *in vivo* conditions (Fig. 9).

Strong ($R = 0.81$) and significant ($p < 0.0001$) correlation, evaluated for the cavitation metrics, indicates that: i) cavitation dosimetry can be performed and ii) Ca^{2+} SP cytotoxicity can be highly predicted on the metric basis – either by monitoring CD or MB sonodestruction rate. Therefore, MB inertial cavitation can be reasonably controlled, based on the principle of feedback-loop, if supplemented with extensive statistical data. Cavitation control could be interchangeably performed by monitoring side- or back-scattered US signals and selecting US parameters, corresponding to appropriate cavitation metric values.

3.6. Result Summary

Since, we have performed an extensive study, we have summarized our findings in Table 4.

Key scientific advancements in the field are summarized below:

1. Comprehensive study on Ca^{2+} SP across cell suspension, 3-D spheroid and tumor models:
   - o Previous works focused mainly on Ca^{2+} EP or single-model *in vitro* Ca^{2+} SP research.
   - o Study provides a multi-level validation – spanning from cell suspension to spheroid to animal models.
2. Rapid and pronounced cytotoxicity due to Ca^{2+} intracellular delivery:
   - o Even at low acoustic pressure and without MB application, Ca^{2+} induced cell death on the level of BLM in cell suspension setting.
   - o Ca^{2+} SP showed rapid onset of action (within 15 min) – rare for conventional chemotherapeutics.
   - o In spheroid and *in vivo* models, Ca^{2+} SP was effective when coupled with MB cavitation.
3. Quantified correlation-based link between cavitation metrics and therapeutic outcome:
   - o Antitumor effectiveness can be obtained even at lower values of cavitation metrics, indicating US- or cavitation-related safety aspects of the treatment.
   - o Strong correlation between cavitation metrics and tumor regression allows for predictive dosimetry using real-time feedback control – important for clinical safety.

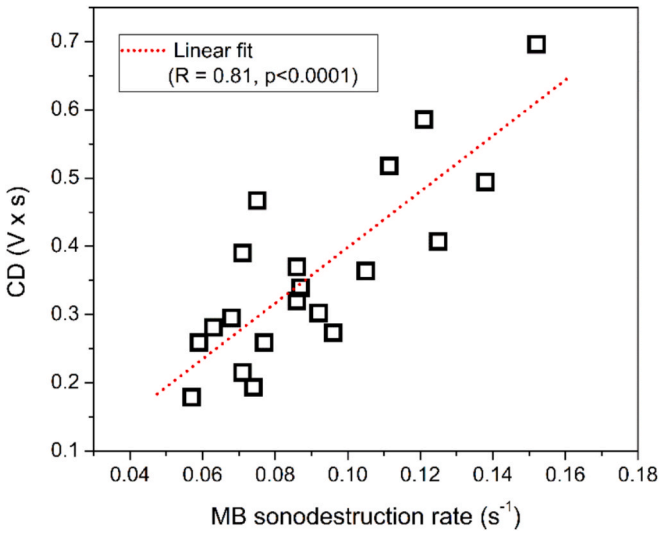

Fig. 9. The correlation between MB sonodestruction rate and CD.

4. Discussion

In this study, we have evaluated the impact of Ca^{2+} SP on murine breast cancer (4 T1) cells in: i) a suspension, ii) spheroid as well as iii) subcutaneous tumor models. Ca^{2+} SP has been determined to be as efficient in cytotoxicity as BLM SP. It was able to diminish the percentage of viable cells down to ~ 10 % in a suspension. Ca^{2+} SP efficiently disrupts three fundamental functions, essential for the viability and expansion of cancer cells. The latter include: cell membrane permeability, metabolic activity and cell proliferation (Figs. 2 and 3). According to the presented data (Fig. 2), 5 mM concentration of Ca^{2+}, even if combined only with US alone (up to 200 kPa acoustic pressure), was sufficient to induce cell death up to ~ 80 %. Indeed, the cytotoxicity of Ca^{2+} was similar to BLM's. These results indicate that Ca^{2+} can be exploited as an effective alternative to conventional BLM against murine breast cancer. Also, this implies significantly less toxic treatment for the patients, since the overload of Ca^{2+} can be well-disposed by cells via intrinsic self-regulation mechanisms [24–28].

Ca^{2+} rapidly (within 15 min) induces damage to 4 T1 cells in a suspension as well as reduces the growth of 3-D cell cultures from the first day. On the contrary, there was no immediate cytotoxic effect of BLM SP for cells in a suspension. Consequently, due to its rapid cell-killing effect, Ca^{2+} SP may be developed into a possible alternative for chemotherapeutic treatment in the long-term. Fast cell death, elicited by Ca^{2+} overload, may be attributed to its high cytoplasmic mobility in the role of a second messenger [21]. Conversely, DNA intercalating agents, such as BLM, slowly migrate to nucleus and require direct binding to nuclear DNA in order to initiate cell mortality [1].

Conversely to our previous studies on Ca^{2+} SP using CHO cells, the efficient anticancer effect for 4 T1 cells was obtained without MBs at relatively low acoustic pressure (≤200 kPa). Ca^{2+} + US initiated cell death up to 30 % at 800 kPa, whereas efficient cytotoxicity (~80 %) was only achieved s at 400–500 kPa and in the presence of MBs. However, in those studies, approximately a half of the cell death was attributed to the deleterious effects of MB inertial cavitation [31–33].

Not surprisingly, efficient growth reduction of 3-D cell cultures required stronger cavitation activity than cells in a suspension. Ca^{2+} + US (400 or 700 kPa) or Ca^{2+} + MB + US (400 kPa) were capable to suppress the spheroid growth around its initial size. However, only Ca^{2+} SP at 700 kPa acoustic pressure was able to induce significant ($p < 0.05$) spheroid regression from the first day after the treatment. Spheroid models simulate some features, characteristic for tumor microenvironment, such as cell-to-cell interaction as well as permeability/diffusion barrier. However, they do not incorporate healthy neighboring cells, lack tumor vasculature or innate immunity-related processes. Furthermore, Ca^{2+} was homogeneously distributed in the spheroid milieu. Since these aspects greatly influence Ca^{2+} intracellular delivery and consequential biological response, we have eventually shifted to *in vivo* tumor models.

In vivo research have shown that Ca^{2+} is as efficient as BLM in the treatment of subcutaneous 4 T1 breast cancer (analogue of human breast

Table 4
Summary of the results, obtained in the study.

Model Type	Treatment Conditions	US Parameters	Key Observations	Take-Home Message
4 T1 cells in a suspension	Ca^{2+} (5 mM) or BLM (20 nM) ± MBs	1 MHz, 50–200 kPa, 10 % duty cycle, 6 s	US-induced Ca^{2+} delivery elicited rapid cell death even without MB application. Stronger and faster cytotoxic efficiency than BLM-induced	Ca^{2+} is a fast-acting alternative effectively reducing 4 T1 cell viability in a suspension
3-D cell culture (spheroids)	Ca^{2+} (5 mM) ± MBs	1 MHz, 400 or 700 kPa, 10 % duty cycle, 6 s	Only Ca^2 SP at higher acoustic pressure (700 kPa) significantly reduced spheroid growth	US-driven MB cavitation is essential for Ca^{2+}-induced regression in spheroid size
***In vivo* (subcutaneous murine breast cancer tumors)**	Ca^{2+} (150 mM, intra-tumoral) or BLM (450 μM, intra-venous) ± MBs	0.95 MHz CW, 2 W/cm^2, 60 s	Both Ca^{2+} SP and BLM SP significantly reduced tumor volume and prolonged animal survival up to one month	Ca^{2+} SP is as effective as BLM SP to induce subcutaneous tumor regression in murine models
Cavitation analysis	Passive cavitation detection and B-scan tumor imaging	–	MB sonodestruction and CD strongly correlated with tumor decrease rate ($R > 0.9$, $p < 0.001$)	Slower but efficient antitumor effect was obtained at lower values of cavitation metrics, indicating controlled treatment

cancer stage IV). Again, this shows that Ca^{2+} EP can be a promising therapeutic technique for breast cancer treatment. Indeed, the objective response of the recipients of Ca^{2+} EP had no significant difference compared to the recipients of electro-chemotherapy (using BLM) in human trials [24,25]. Also, Ca^{2+} EP has been reported to have minimal [24,25] or less side-effects, if compared to electro-chemotherapy [26,28]. Fast cell death, induced by Ca^{2+} SP, has the potential to become a complementary adjunct or an alternative for the types of cancer, characterised by fast growth rate. The latter include highly metastatic types of cancer as well as tumors having low doubling time. However, the suppression of fast-spreading cancers, such as breast, kidney or pancreatic, by rapidly retarding its dissemination into secondary sites, is more reasonable. Primarily, because tumor doubling time of breast, lung or pancreatic cancers was reported to be within 10-100ths of days [48–50].

During animal trials, Ca^{2+} was administered via intratumoral injection, creating local Ca^{2+} gradients within the tumor. Yet, the treatment still succeeded – indicating the robustness of the therapeutic approach, even with less ideal distribution. In overall, multi-level validation of Ca^{2+} SP, which resulted in the alignment of therapeutic trends across cell, spheroid and tumor models, enhanced the translational capabilities. While direct injection of Ca^{2+} into the tumors was possible due to subcutaneous tumor location, we acknowledge this limitation of Ca^{2+} SP in its current state of the art. This hinders direct translation to the treatment for deep-seated tumors or deeply located early-staged breast cancer nodules. However, therapeutic feasibility of Ca^{2+} SP may be more evident for cutaneous metastases or superficial advanced-stage breast cancer tumors, rather than deep-seated primary tumors. Since Ca^{2+} was injected locally, rather than administered systemically, Ca^{2+} SP could complement to a systemic therapy or surgical tumor excision. In particular, this would be beneficial for inoperable high-stage or palliative cases when cancer treatment, associated with lower systemic toxicity, is preferred. In addition, Ca^{2+} overload may induce secondary phenomenon of immunogenic cell death for satellite untreated metastases. Indeed, previous research on Ca^{2+} EP have determined strong tumor regression in untreated cancerous sites, characterised by the accumulation of immune cells [21,51,52]. Therefore, Ca^{2+} SP may enhance systemic anticancer immunity as an adjunct to local therapeutic application.

Correlation analysis has indicated that faster tumor reduction rates were associated with higher values of cumulated CD (Fig. 7J) as well as increased MB sonodestruction rate (Fig. 8C). Spectral data indicated the transition in MB behavior from linear to non-linear pattern, however, the majority of MBs seemed to remain in stable cavitation. This can be attributed to high subharmonical and ultraharmonical increase, simultaneously followed by harmonic decrease (Fig. 7). However, we may assume that inertial cavitation was also occurring at *in vivo* conditions, since we have observed the decrease in interharmonical (1.5–1.75 MHz) RMS curve to 0 V background (Fig. 7F). This tendency highly correlates with MB sonodestruction for *in vitro* setting (Fig. 5E and I). Indeed, the data of B-scan imaging has also indicated MB sonodestruction (Fig. 8B) and was also responsible for observed biological effects. Furthermore, the presence of inertial cavitation may be observed in Fig. 7J and 8C, as higher CD values or MB sonodestruction rates were associated with faster tumor regression.

In general, the retention of oscillating MBs in the mode of stable cavitation is beneficial, since cavitating nuclei induce the permeabilisation of adjacent cells without irreversible membrane damage. On the contrary, inertial cavitation of MBs is associated with MB sonodestruction and the following cell-injurious phenomena, such as shock waves, temperature hot spots or micro-jets. These effects directly increase the death rate of adjacent healthy cells. Due to this reason, cells in a suspension were exposed to pulsed US (1 MHz center frequency, 100–200 kPa peak negative pressure, 10 % duty cycle), resembling low intensity US. Current parameters were selected to minimize possible thermal and off-target mechanical damage, that could be induced by high-pressure US as well as resultant inertial cavitation. Therefore, the impact of US/ cavitation was necessary to be minimized, as we were mostly interested in the effect of intra-cellularly delivered Ca^{2+}. Further transition to spheroid and tumor models, required even more intense pulsed or CW mode US, since they introduced structural barrier for Ca^{2+} entry. These US parameters were previously validated in SP studies to ensure efficient anticancer agent delivery [31–33,44]. However, our results demonstrate that animals were healed even at lower CD values or MB sonodestruction rates, implying that efficient Ca^{2+} SP can be achieved in the presence of low-to-moderate MB cavitation activity.

In the end, we acknowledge that surgical excision is the gold standard for accessible and resectable tumors due to its therapeutic potential. However, in the long-term, Ca^{2+} SP may provide a therapeutic alternative for hardly-accessible or inoperable cancers, such as pancreatic or kidney. Ca^{2+} can be administered locally by performing intratumoral injection, guided in real-time by US or computed tomography imaging. This could enhance the application of repeated treatment strategies and, also, trigger anticancer immunity. Currently, Ca^{2+} SP should not be considered as a stand-alone alternative but rather a complementary option, applicable for specific therapeutic cases.

5. Conclusion

Current study demonstrates that Ca^{2+} SP is a relevant strategy for inducing cytotoxic effects in murine breast cancer models. By delivering Ca^{2+} via US-elicited cavitation, we have achieved significant anticancer effect in: i) 4 T1 cell suspension, ii) 3-D spheroid and iii) *in vivo* subcutaneous tumor models.

Ca^{2+} SP induced rapid (≤15 min) and efficient (>80 %) 4 T1 cell death in a suspension at relatively low 100–200 kPa acoustic pressure, without the application of MBs. However, for 3-D spheroids, efficient growth reduction required higher MB cavitation activity, which was achieved at 700 kPa acoustic pressure.

Ca^{2+} SP was demonstrated to be as effective as conventional BLM-based SP for the suppression of tumor growth and prolonging the survival of laboratory mice. Current therapeutic approach induced

complete tumor eradication, starting from the third day after the treatment, and prolonged animal survival up to one month. Successful treatment of 4 T1 tumors was observed even at low values of cavitation metrics, cavitation dose or MB sonodestruction rate, indicating reliable possibility to overcome US- or cavitation-associated cell or tissue damage.

Current *in vivo* application of Ca^{2+} SP involved direct intratumoral injection of Ca^{2+}. Therefore, translational potential of our method lies in the treatment of subcutaneous tumors or unresectable metastases when surgical intervention is not favored. Future work should validate the efficiency of Ca^{2+} SP on larger animal cohorts, including not only subcutaneous but also deep-seated tumors. Additional assessment of Ca^{2+} SP across diverse cancer types and anatomical locations is essential to fully determine its curative potential and safety aspects prior to clinical translation.

Declarations.

Ethics approval and consent to participate.

The experiments were performed with the permission of the Lithuanian State Food and Veterinary Service (No. G2-149, issued 2020 05–05). M. Maciulevicius has license to work with laboratory animals (No. PK 46564, issued 2023–11-14).

Consent for publication

Not applicable.

Availability of Data and Material.

The datasets generated during and/ or analyzed during the current study are available from the corresponding author on reasonable request.

Institutional Review Board Statement.

Not Applicable.

CRediT authorship contribution statement

Martynas Maciulevičius: Writing – review & editing, Writing – original draft, Visualization, Methodology, Formal analysis, Data curation, Conceptualization. **Reda Rulinskaitė:** Visualization, Methodology, Formal analysis, Data curation, Conceptualization. **Lukas Giedrimas:** Methodology, Data curation. **Rūta Palepšienė:** Methodology, Data curation. **Paulius Ruzgys:** Methodology, Data curation. **Rytis Jurkonis:** Methodology, Data curation. **Mindaugas Tamošiūnas:** Methodology, Data curation, Conceptualization. **Renaldas Raišutis:** Methodology, Funding acquisition. **Kristine Saleniece:** Methodology, Funding acquisition. **Saulius Šatkauskas:** Methodology, Funding acquisition, Conceptualization.

Funding

This work was supported by the grant: “The development of controlled cancer treatment modality based on Ca^{2+} delivery via ultrasound (S-PD-22–51)” from the Research Council of Lithuania. Also, supported by the grant “S-MIP-23–124” from the Research Council of Lithuania.

Declaration of competing interest

The authors declare that they have no known competing financial interests or personal relationships that could have appeared to influence the work reported in this paper.

References

[1] J.P. Brandt, V. Gerriets, Bleomycin, StatPearls [Internet], StatPearls Publishing, Treasure Island (FL), 2021. pubmed.ncbi.nlm.nih.gov/32310355/.
[2] K. Johnson-Arbor, R. Dubey, Doxorubicin, StatPearls [Internet], StatPearls Publishing, Treasure Island (FL), 2023. pubmed.ncbi.nlm.nih.gov/29083582/.
[3] L. Khoja, A. McGurk, C. O’Hara, S. Chow, J. Hasan, Mortality within 30 days following systemic anti-cancer therapy: a review of all cases over a 4-year period in a tertiary cancer centre, Eur. J. Cancer 51 (2015) 233–240, https://doi.org/10.1016/j.ejca.2014.11.011.
[4] J. Qin, T.Y. Wang, J.K. Willmann, Sonoporation: applications for cancer therapy, Advances in Experimental Medicine and Biology 880 (2016) 263–291, https://doi.org/10.1007/978-3-319-22536-4_15.
[5] S. Kotopoulis, A. Delalande, M. Popa, V. Mamaeva, G. Dimcevski, O.H. Gilja, M. Postema, B.T. Gjertsen, E. McCormack, Sonoporation-enhanced chemotherapy significantly reduces primary tumour burden in an orthotopic pancreatic cancer xenograft, Mol. Imaging Biol. 16 (2014) 53–62, https://doi.org/10.1007/s11307-013-0672-5.
[6] H.L. Liu, M.Y. Hua, P.Y. Chen, P.C. Chu, C.H. Pan, H.W. Yang, C.Y. Huang, J. J. Wang, T.C. Yen, K.C. Wei, Blood-brain barrier disruption with focused ultrasound enhances delivery of chemotherapeutic drugs for glioblastoma treatment, Radiology 255 (2010) 415–425, https://doi.org/10.1148/radiol.10090699.
[7] C.Y. Ting, C.H. Fan, H.L. Liu, C.Y. Huang, H.Y. Hsieh, T.C. Yen, K.C. Wei, C.K. Yeh, Concurrent blood-brain barrier opening and local drug delivery using drug-carrying microbubbles and focused ultrasound for brain glioma treatment, Biomaterials 33 (2012) 704–712, https://doi.org/10.1016/j.biomaterials.2011.09.096.
[8] R. Suzuki, E. Namai, Y. Oda, N. Nishiie, S. Otake, R. Koshima, K. Hirata, Y. Taira, N. Utoguchi, Y. Negishi, S. Nakagawa, K. Maruyama, Cancer gene therapy by IL-12 gene delivery using liposomal bubbles and tumoral ultrasound exposure, J. Control. Release 142 (2010) 245–250, https://doi.org/10.1016/j.jconrel.2009.10.027.
[9] C. Pu, S. Chang, J. Sun, S. Zhu, H. Liu, Y. Zhu, Z. Wang, R.X. Xu, Ultrasound-mediated destruction of LHRHa-targeted and paclitaxel-loaded lipid microbubbles for the treatment of intraperitoneal ovarian cancer xenografts, Mol. Pharm. 11 (2014) 49–58, https://doi.org/10.1021/mp400523h.
[10] A.G. Sorace, J.M. Warram, H. Umphrey, K. Hoyt, Microbubble-mediated ultrasonic techniques for improved chemotherapeutic delivery in cancer, J. Drug Target 20 (2012) 43–54, https://doi.org/10.3109/1061186X.2011.622397.
[11] Y.Z. Zhao, D.D. Dai, C.T. Lu, H.F. Lv, Y. Zhang, X. Li, W.F. Li, Y. Wu, L. Jiang, X. K. Li, P.T. Huang, L.J. Chen, M. Lin, Using acoustic cavitation to enhance chemotherapy of DOX liposomes: experiment in-vitro and in-vivo, Drug Dev. Ind. Pharm. 38 (2012) 1090–1098, https://doi.org/10.3109/03639045.2011.640332.
[12] P. Haag, F. Frauscher, J. Gradl, A. Seitz, G. Schafer, J.R. Lindner, A.L. Klibanov, G. Bartsch, H. Klocker, I.E. Eder, Microbubble-enhanced ultrasound to deliver an antisense oligodeoxynucleotide targeting the human androgen receptor into prostate tumours, J. Steroid Biochem. Mol. Biol. 102 (2006) 103–113, https://doi.org/10.1016/j.jsbmb.2006.09.027.
[13] A. Greco, A. Di Benedetto, C.M. Howard, S. Kelly, R. Nande, Y. Dementieva, M. Miranda, A. Brunetti, M. Salvatore, L. Claudio, D. Sarkar, P. Dent, D.T. Curiel, P. B. Fisher, P.P. Claudio, Eradication of therapy-resistant human prostate tumors using an ultrasound-guided site-specific cancer terminator virus delivery approach, Mol. Ther. 18 (2010) 295–306, https://doi.org/10.1038/mt.2009.252.
[14] K. Yamaguchi, L.B. Feril Jr., K. Tachibana, A. Takahashi, M. Matsuo, H. Endo, Y. Harada, J. Nakayama, Ultrasound-mediated interferon β gene transfection inhibits growth of malignant melanoma, Biochem. Biophys. Res. Commun. 411 (2011) 137–142, https://doi.org/10.1016/j.bbrc.2011.06.115.
[15] Z. Fan, R.E. Kumon, J. Park, C.X. Deng, Intracellular delivery and calcium transients generated in sonoporation facilitated by microbubbles, J. Control. Release 142 (2010) 31–39, https://doi.org/10.1016/j.jconrel.2009.09.031.
[16] R.E. Kumon, M. Aehle, D. Sabens, P. Parikh, Y.W. Han, D. Kourennyi, C.X. Deng, Spatiotemporal effects of sonoporation measured by real-time calcium imaging, Ultrasound Med. Biol. 35 (2009) 494–506, https://doi.org/10.1016/j.ultrasmedbio.2008.09.003.
[17] I. Beekers, F. Mastik, R. Beurskens, P.Y. Tang, M. Vegter, A.F.W. van der Steen, N. de Jong, M.D. Verweij, K. Kooiman, High-resolution imaging of intracellular calcium fluctuations caused by oscillating microbubbles, Ultrasound Med. Biol. 46 (2020) 2017–2029, https://doi.org/10.1016/j.ultrasmedbio.2020.03.029.
[18] B. Helfield, X. Chen, S.C. Watkins, F.S. Villanueva, Transendothelial perforations and the sphere of influence of single-site sonoporation, Ultrasound Med. Biol. 46 (2020) 1686–1697, https://doi.org/10.1016/j.ultrasmedbio.2020.02.017.
[19] E. Memari, F. Hui, H. Yusefi, B. Helfield, Fluid flow influences ultrasound-assisted endothelial membrane permeabilization and calcium flux, J. Control. Release 358 (2023) 333–344, https://doi.org/10.1016/j.jconrel.2023.05.004.
[20] S.K. Frandsen, J. Gehl, A review on differences in effects on normal and malignant cells and tissues to electroporation-based therapies: a focus on calcium electroporation, Technol. Cancer Res. Treat. 17 (2018) 1533033818788077, https://doi.org/10.1177/1533033818788077.
[21] S.K. Frandsen, M. Vissing, J. Gehl, A comprehensive review of calcium electroporation—A novel cancer treatment modality, Cancers 12 (2020) 290, https://doi.org/10.3390/cancers12020290.
[22] E.L. Hansen, E.B. Sozer, S. Romeo, S.K. Frandsen, P.T. Vernier, J. Gehl, Dose-dependent ATP depletion and cancer cell death following calcium electroporation: relative effect of calcium concentration and electric field strength, PLoS One 10 (2015) e0122973, https://doi.org/10.1371/journal.pone.0122973.
[23] S.K. Frandsen, H. Gissel, P. Hojman, T. Tramm, J. Eriksen, J. Gehl, Direct therapeutic applications of calcium electroporation to effectively induce tumor necrosis, Cancer Res. 72 (2012) 1336–1341, https://doi.org/10.1158/0008-5472.CAN-11-3782.
[24] H. Falk, L.W. Matthiessen, G. Wooler, J. Gehl, Calcium electroporation for treatment of cutaneous metastases: a randomized double-blinded phase II study comparing the effect of calcium electroporation with electrochemotherapy, Acta Oncol. 57 (2018) 311–319, https://doi.org/10.1080/0284186X.2017.1355109.

[25] D. Agoston, E. Baltás, H. Ócsai, S. Rátkai, P.G. Lázár, I. Korom, E. Varga, I. B. Németh, É. Dósa-Rácz Viharosné, J. Gehl, J. Oláh, L. Kemény, E.G. Kis, Evaluation of calcium electroporation for the treatment of cutaneous metastases: a double-blinded randomised controlled phase II trial, Cancers (Basel) 12 (2020) 179, https://doi.org/10.3390/cancers12010179.

[26] M. Vissing, M. Pervan, J. Pløen, M. Schnefeldt, S.R. Rafaelsen, L.H. Jensen, A. Rody, J. Gehl, Calcium electroporation in cutaneous metastases: a non-randomised phase II multicentre clinical trial, Eur. J. Surg. Oncol. (2023), https://doi.org/10.1016/j.ejso.2023.04.024.

[27] M. Vissing, J. Ploen, M. Pervan, K. Vestergaard, M. Schnefeldt, S.K. Frandsen, S. R. Rafaelsen, C.L. Lindhardt, L.H. Jensen, A. Rody, J. Gehl, Study protocol designed to investigate tumour response to calcium electroporation in cancers affecting the skin: a non-randomised phase II clinical trial, BMJ Open 11 (2021) e046779, https://doi.org/10.1136/bmjopen-2020-046779.

[28] C.C. Plaschke, J. Gehl, H.H. Johannesen, B.M. Fischer, A. Kjaer, A.F. Lomholt, I. Wessel, Calcium electroporation for recurrent head and neck cancer: a clinical phase I study, Laryngoscope Investig. Otolaryngol. 4 (2019) 49–56, https://doi.org/10.1002/lio2.233.

[29] J. Rudno-Rudzińska, W. Kielan, M. Guziński, J. Kulbacka, Effects of calcium electroporation, electrochemotherapy, and irreversible electroporation on quality of life and progression-free survival in patients with pancreatic cancer: IREC clinical study, Adv. Clin. Exp. Med. 30 (2021) 765–770, https://doi.org/10.17219/acem/139917.

[30] J. Rudno-Rudzińska, W. Kielan, M. Guziński, M. Płochocki, A. Antończyk, J. Kulbacka, New therapeutic strategy: personalization of pancreatic cancer treatment—irreversible electroporation (IRE), electrochemotherapy (ECT) and calcium electroporation (CaEP) – a pilot preclinical study, Surg. Oncol. 38 (2021) 101634, https://doi.org/10.1016/j.suronc.2021.101634.

[31] M. Maciulevičius, R. Raišutis, B. Jakštys, L. Svilainis, A. Chaziachmetovas, S. Šatkauskas, The assessment of calcium and bleomycin cytotoxic efficiency in relation to cavitation dosimetry, Pharmaceutics 15 (2023) 1463, https://doi.org/10.3390/pharmaceutics15051463.

[32] M. Maciulevičius, R. Palepšienė, S. Vykertas, R. Raišutis, A. Rafanavičius, T. Krilavičius, S. Šatkauskas, The comparison of the dynamics of Ca^{2+} and bleomycin intracellular delivery after cell sonoporation and electroporation in vitro, Bioelectrochemistry 158 (2024) 108708, https://doi.org/10.1016/j.bioelechem.2024.108708.

[33] M. Maciulevičius, D. Navickaitė, S. Chopra, B. Jakštys, S. Šatkauskas, Sudden cell death induced by Ca^{2+} delivery via microbubble cavitation, Biomedicines 9 (2021) 32, https://doi.org/10.3390/biomedicines9010032.

[34] M. Maciulevičius, M. Tamošiūnas, R. Jurkonis, M.S. Venslauskas, S. Šatkauskas, Analysis of metrics for molecular sonotransfer in vitro, Mol. Pharm. 12 (2015) 3620–3627, https://doi.org/10.1021/acs.molpharmaceut.5b00347.

[35] M. Maciulevičius, M. Tamošiūnas, B. Jakštys, R. Jurkonis, M.S. Venslauskas, S. Šatkauskas, Investigation of microbubble cavitation-induced calcein release from cells in vitro, Ultrasound Med. Biol. 42 (2016) 2990–3000, https://doi.org/10.1016/j.ultrasmedbio.2016.08.005.

[36] M. Maciulevičius, M. Tamošiūnas, M.S. Venslauskas, S. Šatkauskas, The relation of bleomycin delivery efficiency to microbubble sonodestruction and cavitation spectral characteristics, Sci. Rep. 10 (2020) 7743, https://doi.org/10.1038/s41598-020-64213-y.

[37] M. Maciulevičius, K.A. Tiwari, D. Navickaitė, S. Chopra, S. Šatkauskas, R. Raišutis, Optimization of microbubble side-scattering signal analysis for efficient cavitation dosimetry, Biomed. Signal Process. Control 63 (2021) 102235, https://doi.org/10.1016/j.bspc.2020.102235.

[38] M. Maciulevičius, R. Jurkonis, D. Jakovels, R. Raišutis, M. Tamošiūnas, The evaluation of microbubble concentration using the techniques of optical spectroscopy, Measurement 228 (2024) 114372, https://doi.org/10.1016/j.measurement.2024.114372.

[39] R. Palepšienė, M. Maciulevičius, P. Ruzgys, B. Jakštys, S. Šatkauskas, The influence of calcium ions on the electrotransfer efficiency of plasmid DNA and cell viability, Appl. Sci. 13 (2023) 1983, https://doi.org/10.3390/app13031983.

[40] D. Navickaitė, P. Ruzgys, M. Maciulevičius, G. Dijk, R.P. O'Connor, S. Šatkauskas, $Ca2^{+}$ roles in electroporation-induced changes of cancer cell physiology: from membrane repair to cell death, Bioelectrochemistry 142 (2021) 107927, https://doi.org/10.1016/j.bioelechem.2021.107927.

[41] D. Navickaitė, P. Ruzgys, V. Novickij, M. Jakutavičiutė, M. Maciulevičius, R. Sincevičiūtė, S. Šatkauskas, Extracellular-Ca^{2+}-induced decrease in small molecule electrotransfer efficiency: comparison between microsecond and nanosecond electric pulses, Pharmaceutics 12 (2020) 422, https://doi.org/10.3390/pharmaceutics12050422.

[42] B.A. Pulaski, S. Ostrand-Rosenberg, Mouse 4T1 breast tumor model, Curr. Protoc. Immunol. Chapter 20 (2001) Unit 20.2. DOI: 10.1002/0471142735.im2002s39.

[43] M.M. Jensen, J.T. Jørgensen, T. Binderup, A. Kjær, Tumor volume in subcutaneous mouse xenografts measured by microCT is more accurate and reproducible than determined by 18F-FDG-microPET or external caliper, BMC Med. Imaging 8 (2008) 16, https://doi.org/10.1186/1471-2342-8-16.

[44] M. Maciulevičius, M. Tamošiūnas, R. Jurkonis, S. Šatkauskas, Dosimetric assessment of antitumor treatment by enhanced bleomycin delivery via electroporation and sonoporation, Bioelectrochemistry 146 (2022) 108153, https://doi.org/10.1016/j.bioelechem.2022.108153.

[45] W.S. Chen, A.A. Brayman, T.J. Matula, L.A. Crum, Inertial cavitation dose and hemolysis produced in vitro with or without Optison, Ultrasound Med. Biol. 29 (2003) 725–737, https://doi.org/10.1016/s0301-5629(03)00013-9.

[46] R. Jurkonis, N. Lamanauskas, S. Šatkauskas, Estimation of resonance frequency and sonodestruction of SonoVue microbubbles, Arch. Acoust. 40 (2015) 293–300, https://doi.org/10.1515/aoa-2015-0032.

[47] M.X. Tang, R.J. Eckersley, Frequency and pressure dependent attenuation and scattering by microbubbles, Ultrasound Med. Biol. 33 (2007) 164–168, https://doi.org/10.1016/j.ultrasmedbio.2006.07.031.

[48] J. Budczies, M. von Winterfeld, F. Klauschen, M. Bockmayr, J.K. Lennerz, C. Denkert, T. Wolf, A. Warth, M. Diete, I. Anagnostopoulos, W. Weichert, D. Wittschieber, A. Stenzinger, The landscape of metastatic progression patterns across major human cancers, Oncotarget 6 (2015) 570–583, https://doi.org/10.18632/oncotarget.2677.

[49] M. Dahan, D. Hequet, C. Bonneau, X. Paoletti, R. Rouzier, Has tumor doubling time in breast cancer changed over the past 80 years? A Systematic Review, Cancer Med. 10 (2021) 5203–5217, https://doi.org/10.1002/cam4.3939.

[50] E. Mehrara, E. Forssell-Aronsson, H. Ahlman, P. Bernhardt, Specific growth rate versus doubling time for quantitative characterization of tumor growth rate, Cancer Res. 67 (2007) 3970–3975, https://doi.org/10.1158/0008-5472.CAN-06-3822.

[51] M. Vissing, S. Sinius Pouplier, L. Munch Larsen, S. Krog Frandsen, A. Lodin, A. V. Lænkholm, J. Gehl, Immune cell populations in the tumour environment following calcium electroporation for cutaneous metastasis: a histopathological study, Acta Oncol. 63 (2024) 398–410, https://doi.org/10.2340/1651-226X.2024.19462.

[52] P. Ruzgys, D. Navickaitė, R. Palepšienė, D. Uždavinytė, N. Barauskaitė, V. Novickij, I. Girkontaitė, B. Šitkauskienė, S. Šatkauskas, Induction of bystander and abscopal effects after electroporation-based treatments, Cancers (Basel) 14 (2022) 3770, https://doi.org/10.3390/cancers14153770.